Supporting Information

Carrow et al. 10.1073/pnas.1716164115

SI Materials and Methods

Nanosilicate Characterization. Synthetic clay nanosilicates (Laponite XLG, $Na^{+}_{0.7}[(Mg_{5.5}Li_{0.3}Si_8O_{20}(OH)_4]^{-}_{0.7}$) were obtained from BYK Additives. Authentication was performed by determining chemical composites, crystal structure, size, and shape of nanosilicates. Specifically, inductively coupled plasma mass spectrometry (ICP-MS) (elemental analysis; NexION 300D; PerkinElmer) and X-ray photoelectron spectroscopy (XPS) (Omicron XPS system with Argus detector) was used to determine chemical composition of nanosilicates. For ICP-MS, nanosilicates was dissolved in 0.5% hydrogen peroxide solution for 24 h. ICP-MS analysis was performed to determine the concentrations of Si, Li, and Mg. Dried nanosilicates were used for XPS analysis, where binding energies for magnesium (Mg *2s*, *2p*), sodium (Na *1s*), oxygen (O *1s*), lithium (Li *1s*), and silicon (Si *2p*) were determined. The raw values were deconvoluted via Lorentzian function using GraphPad Prism. X-ray diffraction (XRD) (Bruker D8 Advanced) was used to determine crystalline structure of nanosilicates. XRD was performed with a copper source on both powdered nanosilicates and exfoliated nanosilicates (in water) that were then flash-frozen in liquid nitrogen and lyophilized. Atomic force microscopy (AFM) (Bruker Dimension Icon Nanoscope) and transmission electron microscopy (TEM) were performed to determine the size and shape of the nanosilicates. For both AFM and TEM, a dilute solution of exfoliated nanosilicates was placed on silicon substrate or carbon grid. For AFM, nanosilicate thickness was observed via tapping mode, and the data were analysis using Nanoscope Analysis software. For TEM, an accelerating voltage of 200 kV using a JEOL-JEM 2010 (Japan) was used to determine the morphology of nanosilicates. The ζ potential and hydrodynamic size of nanosilicate–FBS solutions were measured with a Zetasizer Nano ZS (Malvern Instrument) furnished with a He–Ne laser at 25 °C. Filtered particles were achieved through utilization of a 0.2-μm filter.

In Vitro Studies: Cytocompatibility, Cell Uptake, and Retention. Human mesenchymal stem cells (hMSCs) were acquired from the Texas A&M Institute for Regenerative Medicine, previously isolated and subsequently expanded from voluntary donors under an institutionally approved tissue recovery protocol. hMSCs were cultured under normal media conditions consisting of α-minimal essential media (alpha-MEM) (HyClone, GE Sciences) with 16.5% FBS (Atlanta Biologicals) and 1% penicillin/streptomycin (100 U/100 μg/mL; Gibco). After every 2–3 d, one-half of the culture media was exchanged for fresh media. Cells were passaged with 0.5% trypsin-EDTA upon reaching confluency of ∼70% and seeded at ∼2,500 cells per cm^2. All experiments were completed with cell populations under P5. Seeded cells were treated with and without nanosilicates (Laponite XLG, $Na^{+}_{0.7}[(Mg_{5.5}Li_{0.3}Si_8O_{20}(OH)_4]^{-}_{0.7}$) solution (50 μg/mL) and cultured for 7 d.

Metabolic activity was monitored via 3-(4, 5-dimethylthiazolyl-2)-2,5-diphenyltetrazolium bromide (MTT) (ATCC) and Alamar Blue (Thermo Scientific) assays, per the manufacturers' protocols. The BD Accuri C6 flow cytometer and a propidium iodide (PI) (40 μg/mL) stain with RNase (100 μg/mL) were used to perform cell cycle analysis following earlier protocol (1). Before seeding, hMSCs were serum starved (only 1% FBS in media) for 24 h to synchronize cell populations and then treated with nanosilicates. After 48 h of exposure, cells treated with various concentrations of nanosilicates were trypsinized and fixed in ice-cold 70% ethanol. Formed cell pellets were washed in PBS, followed by incubation in a PI staining solution at 37 °C for 30 min. Cells were stored at 4 °C until flow cytometer analysis. For endocytosis inhibition analysis by flow cytometry, cells were cultured under normal conditions in six-well plates. Cells were washed three times with PBS and then treated with inhibitors of clathrin-mediated, calveolar-mediated, or macropinocytosis (35 μM chlorpromazine hydrochloride, 10 μM nystatin, or 400 nM wortmannin, respectively) (Sigma-Aldrich) at 37 °C for 30 min. After this pretreatment, silicate nanoparticles fluorescently tagged with Rhodamine B were added to the culture (final concentration, 100 μg/mL) and incubated for a further 60 min. Subsequently, the cells were washed with PBS, trypsinized, and then suspended in cell culture medium. Particle uptake was then analyzed via flow cytometry. Hyperspectral images and data were captured using an Olympus research-grade optical microscope equipped with CytoViva patented enhanced dark-field illumination optics and full-spectrum aluminum halogen source illumination. The system was also equipped with the CytoViva hyperspectral imaging system, producing spectral image files from 400 to 1,000 nm at 2-nm spectral resolution. CytoViva's customized version of ENVI hyperspectral image analysis software was used to quantify the sample's spectral response and conduct any spectral mapping of the sample elements.

For evaluation of reactive oxygen species (ROS) production, the BD Accuri C6 flow cytometer was used. hMSCs were cultured in a 12-well plate to ∼70% confluency, and then treated with an ERK inhibitor (PD184352; 5 μM) for 2 h at 37 °C. Cells were then incubated with dihydroethidium (DHE) (25 μM) for 10 min 37 °C. Then, cells were washed with PBS and treated with 50 μg/mL nanosilicates in phenol-red–free and serum-free media for 2 h at 37 °C. After 2 h, cells were washed with PBS, trypsinized, spun down, and then resuspended in PBS for flow cytometer analysis.

For lysosomal staining and actin staining, hMSCs were cultured in a 12-well plate to ∼70% confluency. hMSCs were treated with 1 μL of CellLight Lysosomes-GFP and incubated overnight at 37 °C for lysosomal staining. Then, hMSCs were treated with rhodamine-labeled nanosilicates for 3 h at 37 °C and later fixed with 2.5% glutaraldehyde. Similarly, for actin staining, hMSCs were treated with nanosilicates for 24 h, and then fixed with 2.5% glutaraldehyde and permeabilized with 0.1% Triton X-100. Phalloidin stain was then added, and samples were incubated for 1 h at 37 °C. The stain was removed and washed with 1× PBS, and then samples were treated with PI/RNase for 30 min at 37 °C. Both lysosomal-stained and actin-stained samples were imaged via a confocal microscope (Nikon). Further tracking of nanosilicates and lysosomal activity was done using the BD Accuri C6 flow cytometer. hMSCs were treated with rhodamine-labeled nanosilicates for 1, 3, and 7 d, and then treated with CellLight Lysosome-GFP overnight. Cells were then washed with PBS, trypsinized, spun down, and resuspended in PBS for analysis.

For investigating nanosilicate dissociation within hMSC culture, ICP-MS (elemental analysis) (NexION 300D; PerkinElmer) was performed. hMSCs were cultured with nanosilicates for 1, 3, and 7 d, and then cells were washed with PBS, trypsinized, spun down, and then resuspended in deionized water. After recentrifugation, the pellet was digested in a 1% nitric acid, 0.5% hydrogen peroxide solution for ICP-MS analysis in which the concentrations of Si, Li, and Mg were determined. This digestion protocol was modified from an earlier study (2).

Whole-Transcriptome Sequencing and Analysis. For total mRNA extraction, cells were cultured until 65% confluent and were subjected to two different media compositions for 1 wk. One subset of cells maintained normal media conditions as a negative control (two replicates); another group was treated with nanosilicates (Laponite XLG, $Na^{+}_{0.7}[(Mg_{5.5}Li_{0.3}Si_8O_{20}(OH)_4]^{-}_{0.7}$) (50 μg/mL) for 48 h (two replicates), after which the media was replaced with normal media for the remaining 5 d. Excess nanosilicates were removed as they are expected to be cleared within 48 h. Upon completion of the week, cells were washed with PBS and pelleted. RNA was isolated and collected via a Roche, High Purity RNA Isolation kit following the manufacturer's protocol. Initial quality of nucleic material (~1.5–2.0 μg) was evaluated using spectrometer absorbance ratios between 280/260 nm around 2.0. Samples were analyzed via a high-output HiSeq platform with TruSeqRNA sample preparation and single-end read length of 125 bases (Charlie Johnson, Genomics and Bioinformatics Service, Texas A&M AgriLife Research, College Station, TX). The sequenced reads were trimmed and aligned to the human genome (hg19) using a RNA-seq aligner, Spliced Transcripts Alignment to a Reference (STAR) (3). STAR is a RNA-seq alignment algorithm specifically designed for alignment of reads generated from spliced RNAs. For the control group, 21,563,695 (uniquely mapped, 20,153,164) and 24,531,989 (uniquely mapped, 22,900,448) sequenced reads successfully aligned to the genome for the two replicates. Similarly, 22,266,394 (uniquely mapped, 20,623,575) and 15,769,384 (uniquely mapped, 14,633,793) reads aligned to the genome for the nanosilicate-treated group for both the replicates. For further analysis, only uniquely mapping reads were utilized. The Reference Sequence (RefSeq) genome annotation the human genome (hg19, GRCh37 Genome Reference Consortium Human Reference 37) obtained from University of California, Santa Cruz, genome browser was utilized for obtaining the gene definition. The gene models can also be obtained by using the Bioconductor package GenomicFeatures in R environment (4). Expression of a gene was determined by counting the number of uniquely mapped reads overlapping the coding exons normalized by gene length in reads per kilobase per million (RPKM). We utilized the RPKM measure only to filter the expressed genes. The distribution of expression of genes in each sample shows that 1 RPKM is a reasonable cutoff to remove the genes with no or minimal expression (Fig. S4). Genes >1 RPKM were considered to be expressed in any condition if they were expressed in both the replicates. Genes expressed in at least one of the condition were then tested for differential expression. Generalized linear models (GLMs) were used to identify the differentially expressed genes where the expression counts were modeled as negative binomial distribution (5). The bioconductor package DESeq was used for this purpose. All analyses were done in R. The GO enrichment analysis was done using GOStats bioconductor package. REVIGO (6) was used to refine the extensive list of significant CC GO terms. It reduces the functional redundancies and clusters the terms based on semantic similarity measures. Visualization of gene networks was accomplished through Cytoscape (7) and GeneMANIA (8) and ClueGO (9) by direct comparisons to the reference genome. DAVID Bioinformatics Resources were also utilized for genetic network analysis (10). Only genes with a P adjusted value (Benjamini–Hochberg false-discovery rate) < 0.05 were included within the network and subsequent GO enrichment analysis.

RNA-seq Validation Using qRT-PCR and Western Blot. For qRT-PCR, cells were cultured under similar conditions as RNA-seq. Following RNA isolation, cDNA was synthesized from 1 μg of RNA for each sample via SuperScript III Reverse Transcriptase (Thermo Fisher) following manufacturer's protocol. Primers were designed via NCBI/Primer-BLAST and quality checked via Integrated DNA Technologies' OligoAnalyzer. The following primers were designed and used: *GAPDH* (forward: 5′-CCTTCATTGACCTCAACTACATGG-3′; reverse: 5′-TGGAAGATGGTGATGGGATTTCC-3′), *COMP* (forward: 5′-AACAGTGCCCAGGAGGAC-3′; reverse: 5′-TTGTCTACCACCTTGTCTGC-3′), *ACAN* (forward: 5′-AAGGGCGAGTGGAATGATGT-3′; reverse: 5′-CGTTTGTAGGTGGTGGCTGTG-3′), *CLTCL1* (forward: 5′-TTTTGGCAGGTCAGGCATCC-3′; reverse: 5′-ACCTGTGCTTTCCCAAGACT-3′), *COL11A1* (forward: 5′-GACTATCCCCTCTTCAGAACTGTTAAC-3′; reverse: 5′-CTTCTATCAAGTGGTTTCGTGGTTT-3′), and *TXNIP* (forward: 5′-ACACATGGTGCTCTTCAGGG-3′; reverse: 5′-AGTTGGTATATGCAACAAGCCA-3′). SYBR Green reagent was then used for amplification quantification. Expression and fold change values were calculated from fluorescence using the program DART-PCR (11). For Western blot analysis, cells were cultured under similar conditions as qRT-PCR and RNA-seq. Protein samples were isolated via a Laemmli buffer (4% SDS, 20% glycerol, 10% 2-mercaptoethanol, 100 mM Tris HCl, and 0.2% bromophenol blue). Gel electrophoresis (Mini Gel Tank; Invitrogen) was performed on protein samples, and subsequent gels were transferred (iBlot 2; Invitrogen) to a nitrocellulose membrane according to the manufacturer's protocol. The membranes were blocked with 5% BSA in PBST (PBS plus 0.1% Tween 20) for 30 min, and then Western processed (iBind; Invitrogen). β-Actin, COMP, p-MEK1/2, and COL1A1 primary antibodies and HRP-conjugated secondary antibodies were purchased from Boster Bio, and incubation was performed per the manufacturer's protocols. Blots were developed (SuperSignal West Pico PLUS Chemiluminescent Substrate; Thermo Fisher) and imaged via LI-COR 3600 C-Digit Blot Scanner. Protein bands were quantified with LI-COR software. The blots were then restored and reblocked with 5% BSA in PBST for further protein analysis.

In Vitro Functional Study. For differentiation studies, hMSCs were treated with either osteogenic (normal media supplemented with 10 mM β-glycerophosphate and 50 μM ascorbic acid) or chondrogenic media (DMEM supplemented with 1% ITS+, 10^{-7} M dexamethasone, and 1 mM sodium pyruvate) with and without nanosilicates. For osteogenic differentiation, samples were fixed with 2.5% glutaraldehyde at 14 and 21 d and stained for alkaline phosphatase [1-Step nitro-blue tetrazolium chloride (NBT)/5-bromo-4-chloro-3′-indolyl phosphate *p*-toluidine salt (BCIP) substrate solution; Thermo Fisher Scientific] and mineralization (Alizarin Red S stain; Electron Microscopy Sciences), respectively. Alizarin Red was quantified via acetic acid extraction and subsequent colorimetric detection (12). For chondrogenic differentiation, samples were fixed with 2.5% glutaraldehyde at various time points, washed with PBS, 1% acetic acid, and then quickly stained with 0.1% Safranin O for 5 min. Samples were washed again with PBS twice and then imaged. For immunostaining, fixed cells were incubated with a 1% BSA in PBST (PBS plus 0.1% Tween 20) for 30 min to block nonspecific binding. Cells were then incubated with a mouse anti-human aggrecan primary antibody (Abcam) within a 1% BSA solution overnight at 4 °C. The primary antibody was then removed and cells were washed with PBS multiple times. Subsequently, cells were incubated for 1 h at room temperature with a goat anti-mouse IgG with conjugated Alexa Fluor 647 (Abcam) in a 1% BSA solution. The secondary antibody was then decanted, and cells were washed multiple times with PBS. Samples were stored in PBS in the dark at 4 °C until imaging.

Statistical Analysis. Statistical analysis was performed via GraphPad Prism software. One-way ANOVA with post hoc Tukey tests was performed. Significant significance values were determined as P values less than 0.5.

1. AshaRani PV, Low Kah Mun G, Hande MP, Valiyaveettil S (2009) Cytotoxicity and genotoxicity of silver nanoparticles in human cells. *ACS Nano* 3:279–290.
2. Figueroa JAL, Stiner CA, Radzyukevich TL, Heiny JA (2016) Metal ion transport quantified by ICP-MS in intact cells. *Sci Rep* 6:20551.
3. Dobin A, et al. (2013) STAR: Ultrafast universal RNA-seq aligner. *Bioinformatics* 29: 15–21.
4. Lawrence M, et al. (2013) Software for computing and annotating genomic ranges. *PLoS Comput Biol* 9:e1003118.
5. Anders S, Huber W (2010) Differential expression analysis for sequence count data. *Genome Biol* 11:R106.
6. Supek F, Bošnjak M, Škunca N, Šmuc T (2011) REVIGO summarizes and visualizes long lists of gene ontology terms. *PLoS One* 6:e21800.
7. Shannon P, et al. (2003) Cytoscape: A software environment for integrated models of biomolecular interaction networks. *Genome Res* 13:2498–2504.
8. Montojo J, et al. (2010) GeneMANIA Cytoscape plugin: Fast gene function predictions on the desktop. *Bioinformatics* 26:2927–2928.
9. Bindea G, et al. (2009) ClueGO: A Cytoscape plug-in to decipher functionally grouped gene ontology and pathway annotation networks. *Bioinformatics* 25:1091–1093.
10. Huang W, Sherman BT, Lempicki RA (2009) Systematic and integrative analysis of large gene lists using DAVID bioinformatics resources. *Nat Protoc* 4:44–57.
11. Peirson SN, Butler JN, Foster RG (2003) Experimental validation of novel and conventional approaches to quantitative real-time PCR data analysis. *Nucleic Acids Res* 31:e73.
12. Gregory CA, Gunn WG, Peister A, Prockop DJ (2004) An Alizarin red-based assay of mineralization by adherent cells in culture: Comparison with cetylpyridinium chloride extraction. *Anal Biochem* 329:77–84.

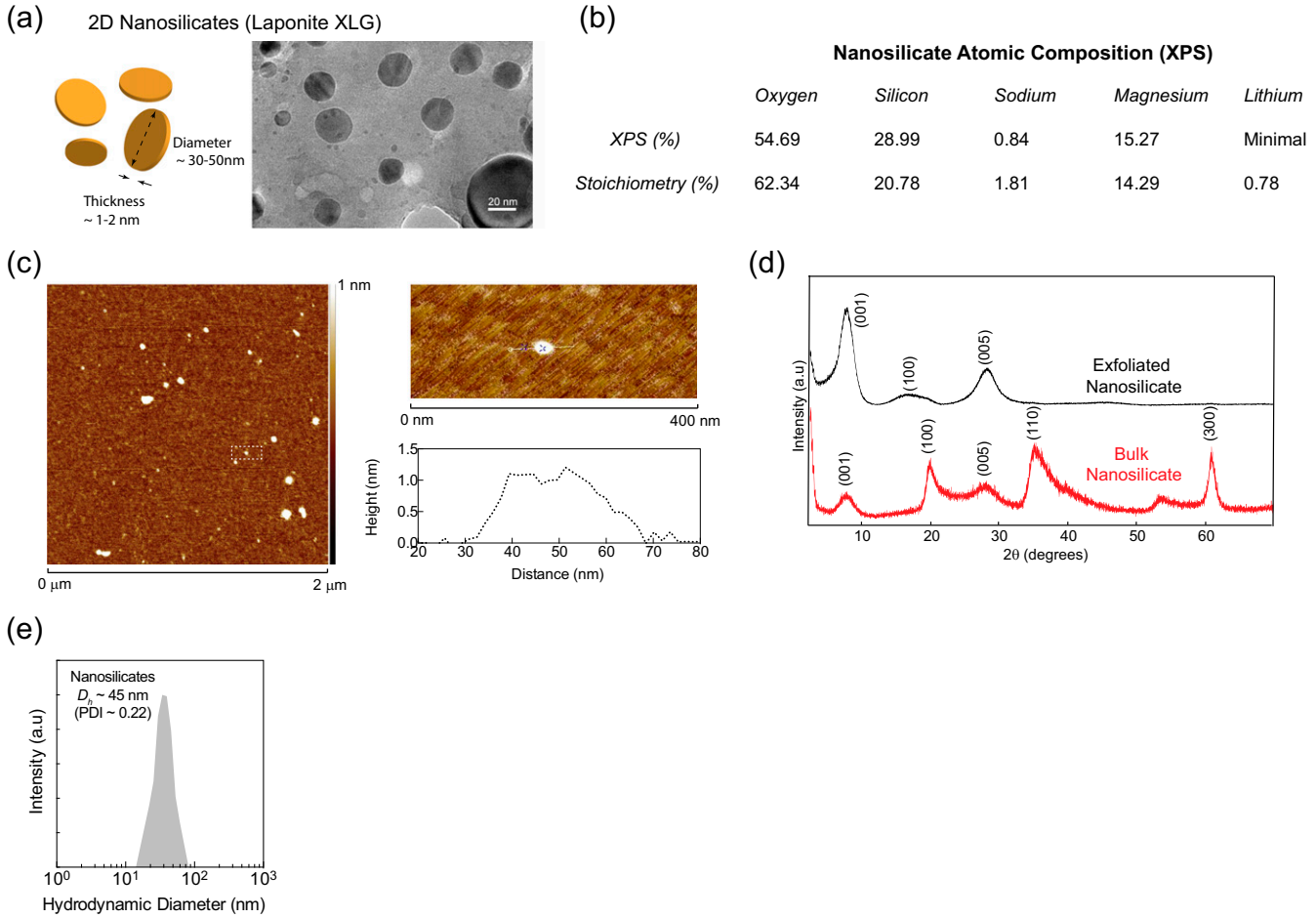

Fig. S1. Physical characterization of nanosilicates was completed to evaluate particles before introducing to hMSCs. (*A*) TEM of nanosilicates demonstrated disk morphology and nanoscale size. (*B*) XPS analysis revealed an elemental composition similar to that of the idealized stoichiometric ratio found within a unit cell of the nanosilicates. (*C*) AFM corroborated the nanoscale diameter (25–50 nm) and thickness (1–1.5 nm) of the nanosilicates. (*D*) XRD of both bulk and exfoliated (flash frozen with subsequent lyophilization) nanosilicates generated peaks at diffraction planes (001), (100), and (005) for both, with (110) and (300) present in the bulk sample. (*E*) DLS measurements quantified variability of nanosilicate hydrodynamic size in particles and displayed a narrow range of diameters (polydispersity index, 0.22) around 45 nm.

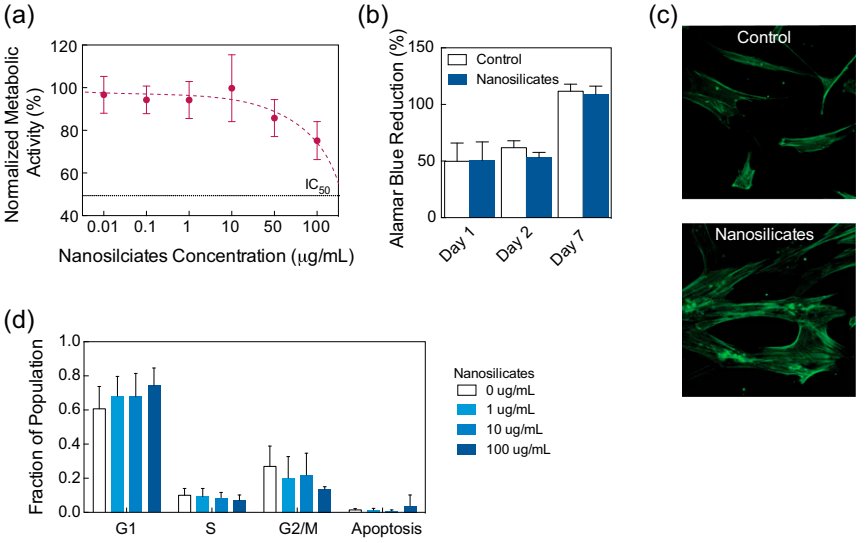

Fig. S2. Nanosilicate effect on cellular processes. (*A*) Metabolic activity, assessed via MTT assay, remained unaffected by nanosilicate introduction at bioactive concentrations. Minimal effect of nanosilicates was observed on cell health monitored via (*B*) Alamar blue assay, (*C*) cytoskeletal organization, and (*D*) cell cycle analysis.

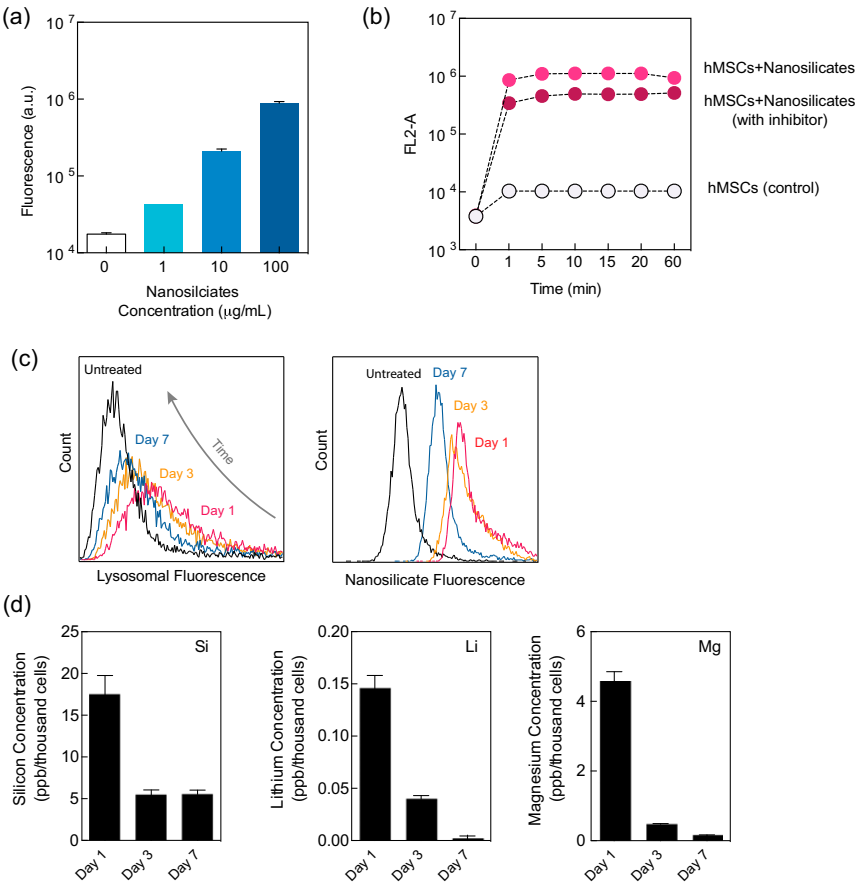

Fig. S3. Nanosilicate interactions with hMSCs were monitored using flow cytometry and ICP-MS. (*A*) Uptake of fluorescently tagged nanosilicates displayed concentration-dependent internalization. (*B*) Endocytosis of particles occurred rapidly with chemical inhibition of a clathrin-mediated process reducing uptake. (*C*) Following internalization, tagged particles were trafficked to lysosomal bodies with an increase in these vesicles observed after 24 h and returning to basal levels over the course of a week. (*D*) Introduction of nanosilicates to low-pH environments of late endosome/lysosome vesicles initiated dissolution of the particles over a week. Ion products were greatest at 24 h and decreased over time as nanosilicates continued to be trafficked in and out of the cell in addition to particle dissociation.

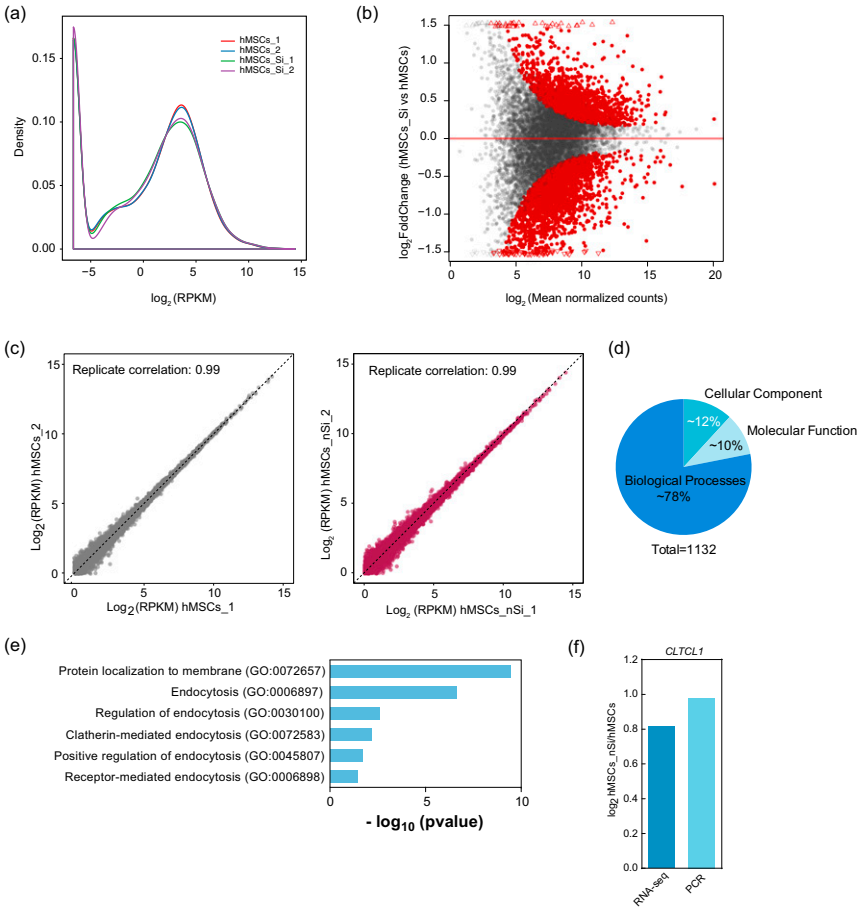

Fig. S4. RNA-seq data analysis. (*A*) Distribution of $\log_2$(RPKM + 0.01) of all genes. (*B*) MA plot (Bland–Altman plot) for the all genes that are tested by the RPKM > 1 cutoff. (*C*) Replicate variation of RNA-seq samples. Correlation for replicates among untreated and treated populations, respectively, indicate high degrees of reliability and consistency between tested samples. (*D*) Broad grouping of GO terms into three main groups: biological processes, cellular component, and molecular function. (*E*) GO terms specific to endocytosis process. (*F*) PCR validation of RNA-seq specific to a gene controlling clathrin machinery [clathrin heavy chain like 1 (*CLTCL1*)].

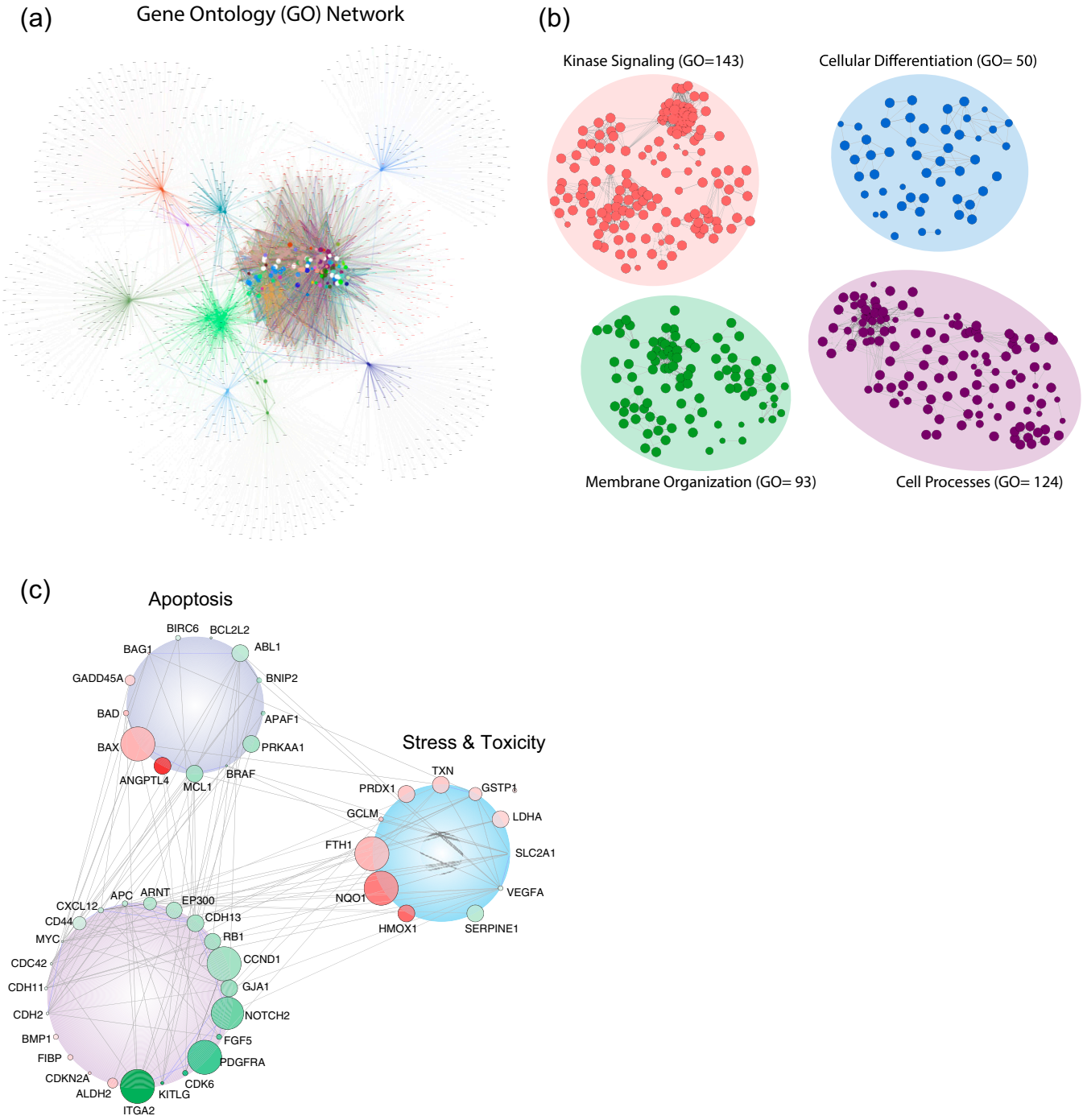

Fig. S5. (*A*) Network of GO terms and expressed gene clusters around each respective correlating term illustrating highly interconnected stimulation with nanosilicates; (*B*) GO terms could be subsequently divided into four primary cellular systems including basic processes, membrane organization, kinase signaling, and differentiation responses; (*C*) gene network displaying interconnected genetic targets after nanosilicate treatment with high degrees of expression and statistical significance (red, up-regulated; green, down-regulated; size increases with significance).

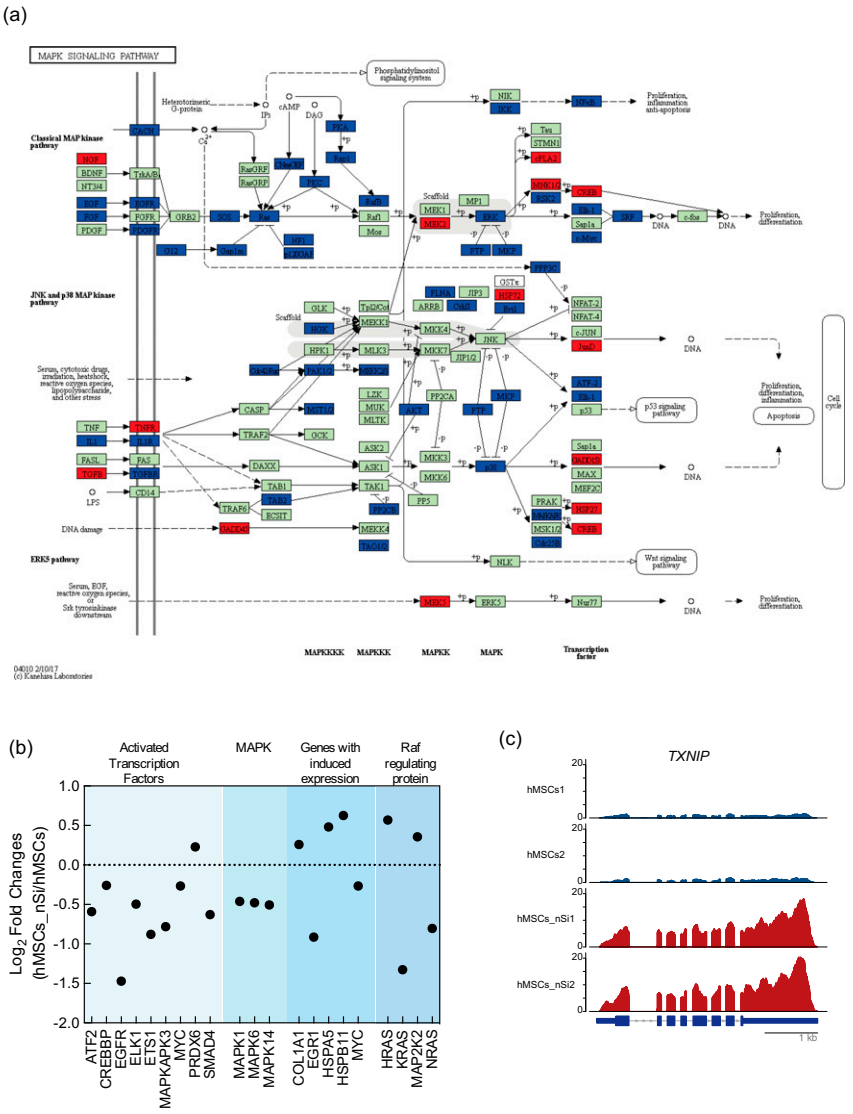

Fig. S6. (*A*) Kegg pathway specific to MAPK signaling with differentially expressed genes from RNA-seq (red, up-regulated; blue, down-regulated). (*B*) Organization of gene expression throughout MAPK signaling pathways. (*C*) Expression tracks of *TXNIP* in hMSCs and nanosilicate-treated hMSCs.

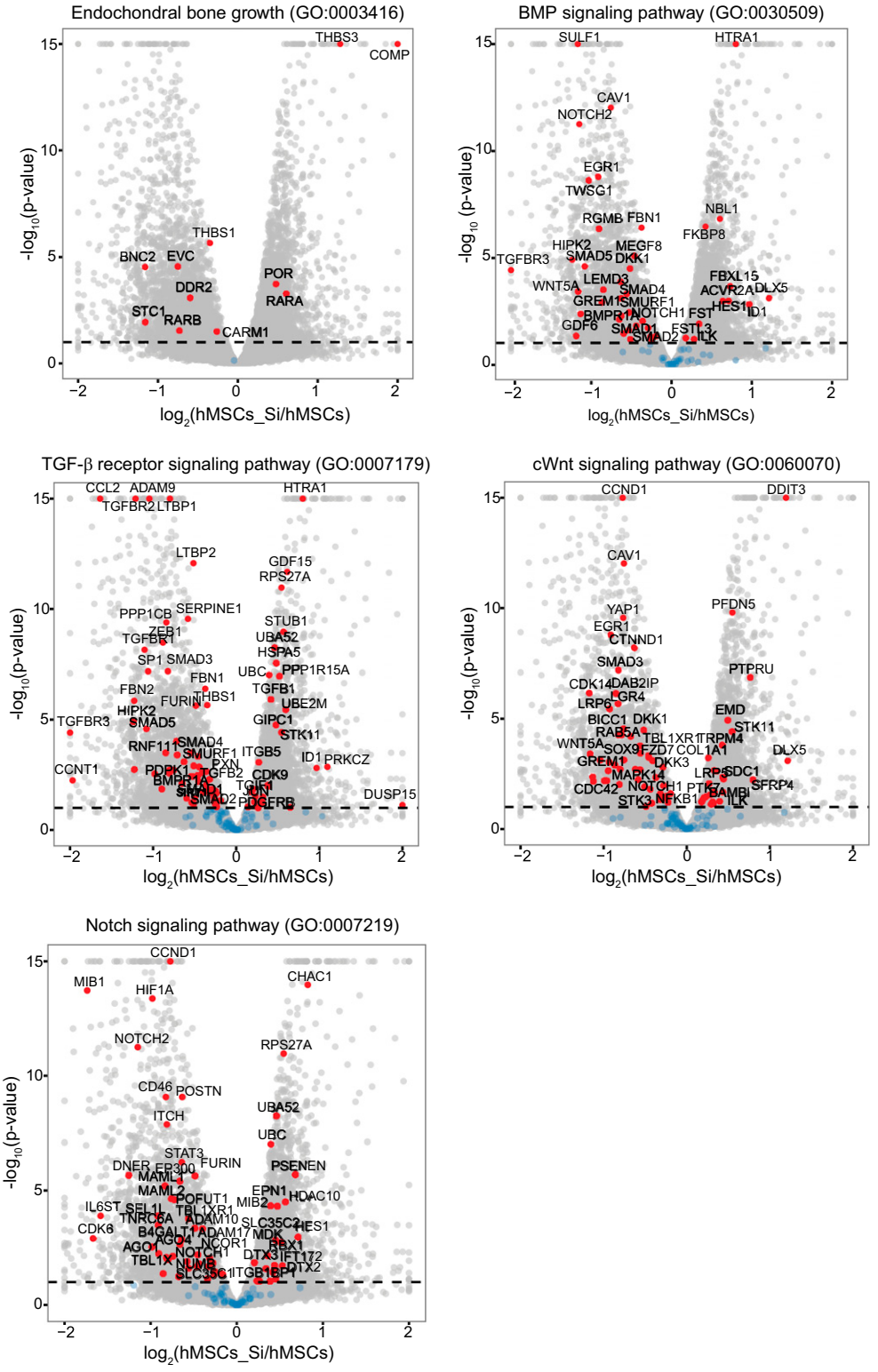

Fig. S7. Volcano plots showing key genes differentially regulated for key GO terms.

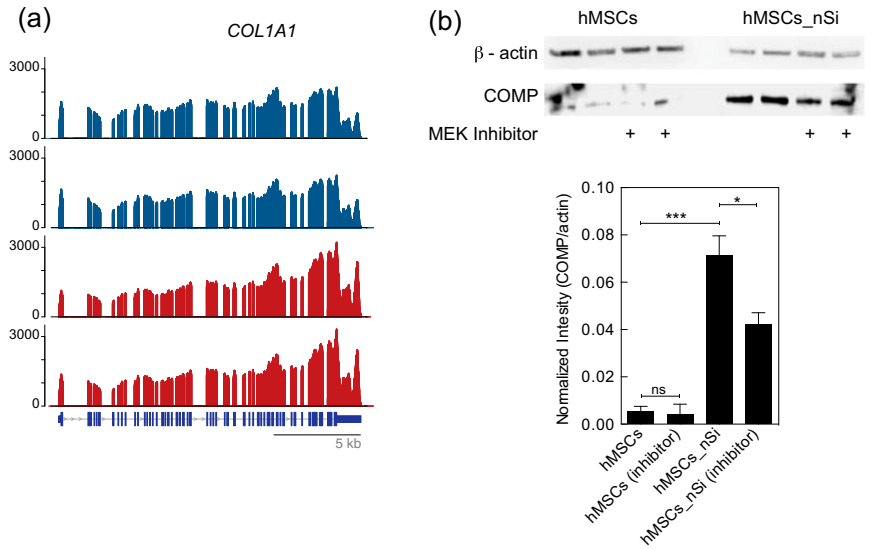

Fig. S8. (*A*) Expression tracks for collagen type I (*COL1A1*) for control (blue) and treated (red) populations. (*B*) Western blot for differentiation-specific proteins, COMP, for control and nanosilicate-treated samples. Addition of a MEK inhibitor reduced protein synthesis of both targets. $*P < 0.05$; $***P < 0.001$. ns, not significant.

Other Supporting Information Files

Dataset S1 (XLS)
Dataset S2 (XLS)
Dataset S3 (XLS)